Research article

Oxygen permeation through perovskitic membranes: The influence of steam in the sweep on the permeation performance

Florian Thaler[*]**, Michael Müller, and Robert Spatschek**

Forschungszentrum Jülich, Institute of Energy and Climate Research – IEK-2, 52425 Jülich, Germany

[*] **Correspondence:** Email: f.thaler@fz-juelich.de; Tel: +49(0)2461-61-1839.

Abstract: Experimental approaches are employed for the understanding of oxygen permeation through membranes. For the experiments, different oxygen partial pressures are applied to both sides of a BSCF5582 membrane, using synthetic air as feed and vacuum or steam/argon as sweep gas. Beside the partial pressure gradient, the permeation rate depends on the temperature and the membrane thickness. Sufficient permeation rates can be achieved by sweeping the membrane with water vapor (steam) instead of a noble gas, which is optimized by ascending water content in the sweep gas. The influence of the steam content on the permeation performance as well as microstructural changes are demonstrated.

1. Introduction

The transport of oxygen and other gases through membranes has a broad range of applications, including the purification of gases, reduction of nitrogen oxides during combustion processes and many other energy and climate relevant purposes.

Especially ion conducting membrane materials are supposed to be the means of choice, when high purity oxygen is required for technical processes like the oxyfuel combustion for carbon capture and storage (CCS) [1] or reactions in chemical industry like the syngas production and hydrogen processing [2]. In comparison to other oxygen production techniques, i.e. the energy-intensive cryogenic air separation (Linde method) or vacuum pressure swing adsorption (VPSA), membrane based methods might be beneficial in terms of decentralized utilizability, combined with a high purity of the produced oxygen. Embedded in a high temperature environment process, oxygen transport membranes (OTMs) are supposed to be an economic alternative to commercial large-industrial processes. Membrane materials with perovskitic structure offer the highest oxygen fluxes due to their mixed ionic and electronic

conductivity (MIEC). Their ability to transport oxygen via vacancies in the crystal lattice enables efficient and highly selective separation of oxygen from ambient air. Such kind of membranes can be applied in several ways, either as separate membrane modules for purified oxygen production or in the form of membrane reactors (MRs) for chemical reactions where oxygen is needed as a reactant. The former could be applicable in modern coal power plants, where the combustion is performed in oxygen enriched atmospheres, whereas oxygen ion conducting MRs are primarily made for the oxidative coupling of methane (OCM) in the syngas generation process ($CH_4 + 0.5 O_2 \rightarrow CO + 2 H_2$). The degradation behavior of those membrane materials is an important issue, since some of the applications implement harsh process conditions concerning oxidizing or reducing atmospheres and flushing with flue gas and steam. The approach in this work consists of a membrane module for oxygen separation from air, whereas the idea is to use steam (water vapor) for sweeping the membrane surface instead of flue gas, since it has been proven that some perovskites decompose under CO_2 containing atmospheres. Especially BSCF ($Ba_xSr_{1-x}Co_yFe_{1-y}O_{3-\delta}$) is prone to form carbonates ($Ba_xSr_{1-x}CO_3$), which impede the oxygen exchange kinetics at the surface and consequently lower the permeation rate through the membrane [3–9]. There are plenty of studies in the literature which have investigated perovskitic hollow fiber membranes operating under steam sweep conditions [10–13]. Most of them show irreversible degradation effects, except the BCFZ ($BaCo_xFe_yZr_zO_{3-\delta}$) membranes described in Wang et al. [10] and the BBCN ($BaBi_{0.05}Co_{0.8}Nb_{0.15}O_{3-\delta}$) fibers from Wang et al. [13]. BSCF and LSCF ($La_xSr_{1-x}Co_yFe_{1-y}O_{3-\delta}$) fibers decompose in the presence of steam, whereas leaching of elements and the rearrangement of the crystalline ordering occurred for both of them. Furthermore, the study of Leo et al. in 2011 [11] verified the formation of a porous carbonate layer on the BSCF fiber membrane surface due to carboxylic acid present in the steam. The work of Wang et al. [12] has proven the stability of LSCF for several 100 hours under varying steam concentrations without a significant deterioration of the permeation performance. So far, there is no clear dependency of the steam content in the sweep on the permeation rate of OTMs reported in the literature. Therefore, the thermochemical stability as well as the permeation performance of such membrane materials under steam containing sweep conditions have to be investigated thoroughly.

2. Materials and Methods

2.1. Perovskite type membrane materials

Perovskites are promising membrane materials for gas separation and generating oxygen from ambient air. Due to their mixed ionic and electronic conductivity (MIEC) and the high amount of oxygen vacancies in the crystal lattice, perovskitic membranes show very high oxygen permeation rates [14, 15] compared to other ion conducting materials in the fluorite structure (AO_2) like yttria doped zirkonia ($Y:ZrO_2$) or gadolinium doped ceria ($Gd:CeO_2$) [16]. All perovskites have a simplified composition $A^{2+}B^{4+}O_3^{2-}$, building a distinct structure type which is named by its natural representative, the mineral perovskite ($CaTiO_3$). Nevertheless, the ideal cubic crystal structure, as illustrated in Fig. 1, is represented by the composition $SrTiO_3$. By means of substituting the A and B positions with other elements, a distortion of the ideal structure occurs. Concurrently, this goes along with an oxygen nonstoichiometry ($\delta \neq 0$) and the formation of oxygen vacancies. The composition consequently is written as $A_{1-x}A'_xB_{1-y}B'_yO_{3-\delta}$, in which cations can be partly substituted by others with different valence and/or ion radius to enhance the ionic and electronic conductivity [17,18]. Well known examples
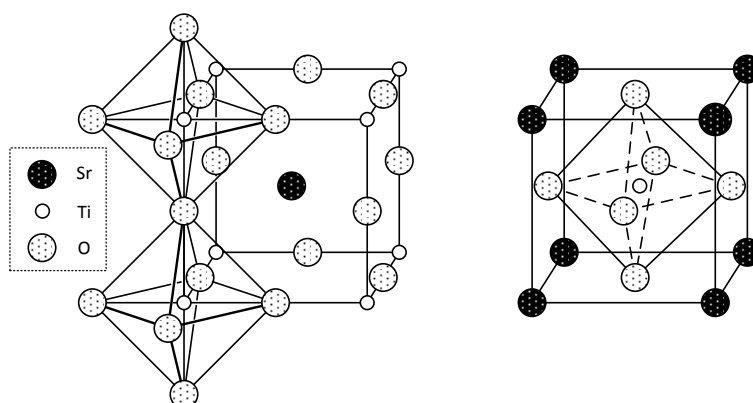
Figure 1. The ideal cubic perovskite structure.

for such perovskitites with high vacancy concentrations are $Ba_{0.5}Sr_{0.5}Co_{0.8}Fe_{0.2}O_{3-\delta}$ (BSCF5582) and $La_{0.6}Sr_{0.4}Co_{0.2}Fe_{0.8}O_{3-\delta}$ (LSCF6428) [19, 20]. BSCF5582 is the subject of the present study, since its materials properties under conventional operating conditions are well known from the literature. This shall set the base for further investigations on the permeation performance in steam sweep conditions.

The so called Goldschmidt tolerance factor, posed in Eq. (1), gives the grade of distortion in the crystal structure of perovskites [21]

$$t = \frac{r_A + r_O}{\sqrt{2}\,(r_B + r_O)}.$$ (1)

Referring to this, r_A and r_B are the cation radii of the A- and B- lattice sites, whereas r_O specifies the oxygen anion radius. Mostly, alkaline-earth or rare-earth elements (e.g. Ca, Sr, Ba, La, Ce, Gd) fill the A sites, whilst the B sites are occupied by transition metals (e.g. Ti, Mn, Fe, Co) for a maximized overall electronic conductivity [18]. A value of $t=1$ is according to the cubic structure without any distortion. Most stable perovskites are found in the range of t=0.8 – 1.0 [22]. A tolerance factor of $t < 1$ induces crystallization in the tetragonal, orthorhombic or rhombohedral crystal system, $t > 1$ stabilizes hexagonal crystals.

2.2. Oxygen transport mechanisms in MIECs

Oxygen transport through MIEC membranes is mainly delimitated by two factors, namely (i) the surface exchange performance at the interfaces between the gas phase and the membrane material and (ii) the bulk diffusion kinetics of oxygen ions via vacancies. If the membrane exceeds a characteristic membrane thickness L_c, bulk diffusion is limiting the overall permeability and the surface exchange rate can be neglected. The transition from gaseous oxygen to the crystal lattice can be expressed using the Kröger-Vink notation (2)

$$V_O^{\bullet\bullet} + \frac{1}{2}O_2 \leftrightarrow O_O^x + 2h^{\bullet}.$$ (2)

One half oxygen molecule needs an oxygen vacancy $V_O^{\bullet\bullet}$ to fill a regular oxygen lattice site O_O^x. Simultaneously two electron holes $h^{\bullet}$ are formed. Assuming that bulk diffusion is dominating, the flux

of oxygen j_{O_2} can be expressed by the Wagner equation (3),

$$j_{O_2} = -\frac{R \cdot T}{16 \cdot F^2 \cdot L} \cdot \int_{\ln p''_{O_2}}^{\ln p'_{O_2}} \frac{\sigma_{el} \cdot \sigma_{ion}}{\sigma_{el} + \sigma_{ion}} \, \mathrm{d} \ln p_{O_2},\tag{3}$$

with the ideal gas constant R, the temperature T, the Faraday constant F, the membrane thickness L, the oxygen partial pressures p'_{O_2} and p''_{O_2} at both sides of the membrane and the partial ionic and electronic conductivities σ_{ion} and σ_{el} [18, 23].
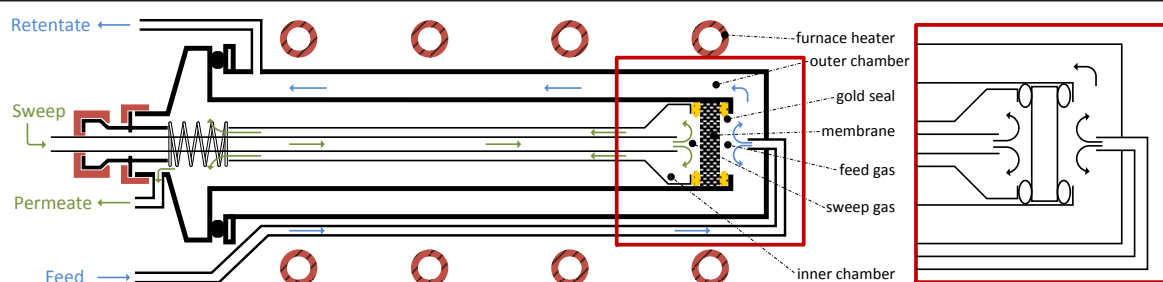
2.3. Permeation measurement setup

At this point we introduce our experimental setup to characterize perovskite type membrane materials concerning their permeability of oxygen at elevated temperatures. Since oxygen needs a chemical potential to migrate through the perivskitic lattice, a preferably high oxygen partial pressure gradient Δp_{O_2} is required. This is permitted, either by sweeping one side of the membrane with a low p_{O_2} gas, e.g. argon, helium and/or water vapor (4-end), or by generating a vacuum on the permeate side (3-end), while feeding the other side with a higher oxygen containing gas like air. Fig. 2 schematically depicts a classical 4-end mode arrangement and explains the common terminology.
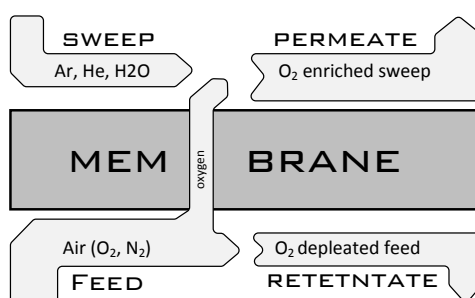
Figure 2. Simplified principle of oxygen permeation through a membrane in 4-end sweep gas mode.

The membranes are fixed in a recipient made of quartz glass (Fig. 3), sealed by two gold rings to separate the gas chambers and to prevent gas exchange. It can hold flat disc membranes of 15 mm in diameter and 0.3 – 5 mm thickness. Either bulk membranes with a single dense ceramic layer, or supported membranes with a very thin functional layer and a porous substrate [15] can be investigated in this setup. In this kind of experiments, oxygen permeates from the outer chamber through the membrane to the inner chamber, where it is swept away by the sweep gas to reach the analyzer unit. The quartz glass recipient is heated in a vertical dual-zone furnace (Prüfer, Neuss DE) up to 1000 °C to soften the gold rings before adding a compressive force via a metal spring. After successful sealing the temperature is reduced to 750 – 900 °C, depending on the material and the given requirements. Temperature is controlled via the furnace heater, assuming a uniform heat distribution in the center of the furnace. The incoming gases are heated on their way through the recipient and the process temperature is reached before entering the membrane surface. The feed gas can be chosen from synthetic air, oxygen, nitrogen, carbon dioxide, helium, argon, Ar/4% H_2, water vapor or a mixture of the named gases. On the other side Ar, He, N_2, O_2 or CO_2 are available as sweep gas. Measurements

Figure 3. Sample holder for oxygen permeation measurements on dense perovskite type membranes.

using water vapor sweep in 4-end mode can be realized by exchanging the feed and sweep side.

For measurements in the so called 3-end mode, an adjustable membrane vacuum pump (*MD 4 NT Vario*, Vacuumbrand GmbH + Co KG, Wertheim DE) can be installed on the permeate side while the sweep inlet is closed. All gas flows are set by mass flow controllers (Brooks Instrument, Hatfield PA USA) in a range of about 20 to 1000 ml min^{-1}, controlled via the *Simatic S7* user interface (Siemens AG, München DE).

2.4. Permeation rate measurement

The permeate gas is analyzed via a mass spectrometer (*OmniStar*, Pfeiffer Vacuum GmbH, Alar DE), equipped with a quadrupole mass analyzer (*Prisma™ QMA 200*) including a Faraday cup detector and an optional secondary electron multiplier (C-SEM). Ionization of the incoming gas molecules is realized by a gas tight ion source with two yttria-coated iridium cathode wires. The quadrupole system uses a high-frequency alternating current voltage to influence the trajectory of the ions in the quadrupole field. Thereby, the ions are separated by means of their mass to charge ratio m/e, and undesirable ions are rejected so that they cannot reach the detector. The Faraday collector counts the incoming ions of defined m/e ratios and transfers the electrical charge into an ion proportional voltage. This ion current is proportional to the amount of the single gas species O_2, N_2 and argon. By calibrating the gas analyzer with a given gas composition, the concentrations $c_{O_2}^{perm}$, $c_{N_2}^{perm}$ and c_{Ar}^{perm} in the permeate stream can be determined. Basically, the oxygen permeation rate through a membrane can be calculated with the determined concentration $c_{O_2}^{perm}$ and the flow rate $\dot{V}^{perm}$ of the permeate gas according to

$$J_{O_2} = \dot{V}^{perm} \cdot c_{O_2}^{perm}. \tag{4}$$

Due to some unavoidable leakage along the circumference of the membrane discs, additional oxygen, which is coming from the feed gas, is entering the permeate side. Assuming that with every N_2 molecule 0.266 molecules O_2 are leaking across the seal (according to the O_2/N_2 ratio of 0.21/0.79 in ambient air), one can correct $c_{O_2}^{perm}$ by subtracting the term

$$c_{O_2}^{leak} = c_{N_2}^{perm} \cdot \frac{c_{O_2}^{feed}}{c_{N_2}^{feed}}. \tag{5}$$

Furthermore, the flow rate of the permeate $\dot{V}^{perm}$ could not be measured directly while operation, but it can be calculated by means of dividing the sweep gas flux $\dot{V}^{sweep}$ by the measured argon concentration c_{Ar}^{perm},

$$\dot{V}^{perm} = \frac{\dot{V}^{sweep}}{c_{Ar}^{perm}}. \tag{6}$$

Moreover, the whole term is divided by the active membrane area A, to make the measurements comparable to other experimental setups which might investigate smaller/larger or even tubular membranes. Combining (4), (5) and (6) we can determine the oxygen permeation rate density j_{O_2} as

$$j_{O_2} = \frac{\dot{V}^{sweep}}{c_{Ar}^{perm}} \cdot \left(c_{O_2}^{perm} - \left(c_{N_2}^{perm} \cdot \frac{c_{O_2}^{feed}}{c_{N_2}^{feed}} \right) \right) \cdot \frac{1}{A}. \tag{7}$$

3. Results and Discussion

3.1. Temperature dependence of permeation in BSCF5582

As mentioned above, the permeability of perovskitic membrane materials strongly depends on the operation temperature T, the membrane thickness L and the oxygen partial pressure gradient $\Delta p_{O_2} = p'_{O_2}/p''_{O_2}$, assuming a bulk diffusion limited kinetics described by the Wagner equation (3). In this study, the oxygen flux j_{O_2} (7) is determined from the measured oxygen and nitrogen concentrations in the sweep gas. To see the temperature dependency, a temperature loop with a bulk membrane of 1 mm thickness is performed in an air-vacuum gradient (3-end mode). The feed gas rate is set to 250 ml min^{-1} synthetic air (0.21% O$_2$/0.79% N$_2$) and a vacuum pressure of 10 mbar is applied on the permeate side to achieve a high Δp_{O_2} ratio. A bypass flux of 140 ml min^{-1} Ar is added to the gas stream after the vacuum pump to dilute the permeated oxygen and to sweep it to the analyzer unit. The samples are prepared by uniaxial pressing of commercial BSCF5582 powder (HITK, Hermsdorf DE) at 25 kN. After sintering at 1000 °C for 12 hours in ambient air, the shape of the membranes is ground to a diameter of about 14.5 mm and the surfaces of both sides are ground and polished to reach exactly 1 mm membrane thickness. The experiment is started at 1000 °C with sealing the membrane within the gold rings in the recipient, before the temperature is reduced slowly with a rate of max. 3.5 K/min to 900 °C, 850 °C, 750 °C and back to 900 °C. At each temperature step, the permeation rate is measured for two hours, to ensure an equilibrated state which is proven by stable ion current values of the selected masses in the MS signal. In Fig. 4 the results for the permeation measurement are depicted in an Arrhenius plot, wherein the oxygen permeance

$$\frac{j_{O_2}}{\ln \left(p'_{O_2} \cdot p''_{O_2}{}^{-1} \right)} \tag{8}$$

as well as the permeation flux j_{O_2} (7) versus the inverse temperature $1000\,K/T$ is plotted. Thereby, the values are corrected by means of the oxygen partial pressure gradient between the feed and the sweep gas side, which is the driving force for the oxygen diffusion. The partial pressures are determined, either from the concentration of oxygen given in the feed (p'_{O_2}=0.21 atm), or for p''_{O_2} from the measured gas concentrations in the permeate. The calculated oxygen partial pressure at the permeate side p''_{O_2} amounts to $2.5 \cdot 10^{-4} - 5.98 \cdot 10^{-4}$ atm. The results show a clear temperature dependency, varying from

0.81 ml min^{-1} cm^{-2} for 900 °C to 0.34 ml min^{-1} cm^{-2} for 750 °C. The plot also shows a slight hysteresis, when the temperature is changed back from 750 °C to 900 °C. A constant nitrogen concentration of 1.7 – 1.8 vol. % measured by the MS for each temperature step may indicate an external leakage at the tubing or the flanges due to the high vacuum pressure in the permeate.
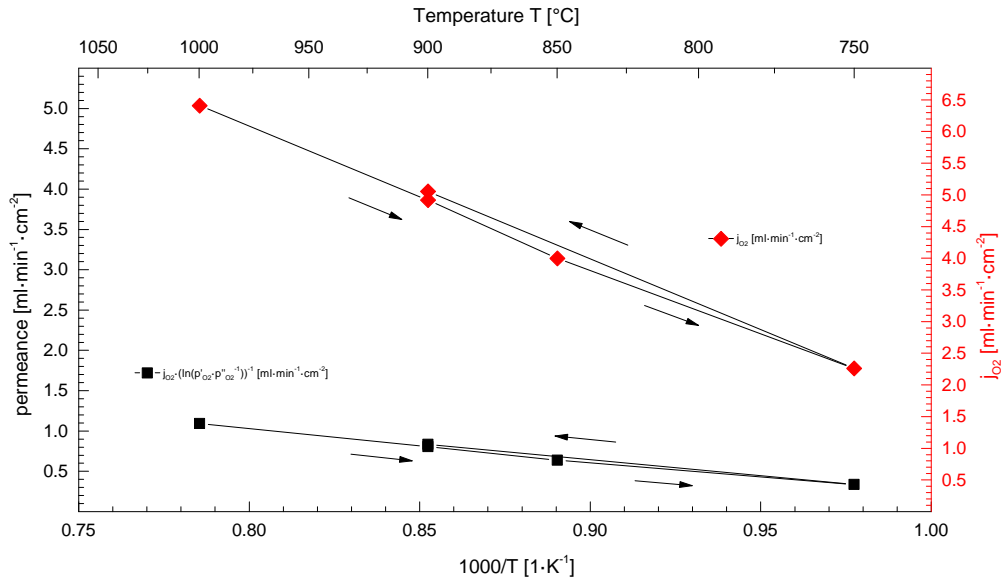
Figure 4. Temperature dependency of the oxygen permeability of a 1 mm thick bulk BSCF5582 membrane measured at a constant pressure gradient in 3-end mode; Arrhenius plot expressing the pemeation flux/permeance versus the inverse temperature.

3.2. Permeation measurements under steam sweep conditions

In an additional part of this study, the influence of a varying content of water vapor in the sweep gas is investigated. Therefore, in a first run water vapor is added to a constant rate of 200 ml min^{-1} argon. The experiment is performed at a constant temperature of 900 °C and 200 ml min^{-1} synthetic air for feed with p'_{O_2} = 0.2 atm. After sweeping the back side of the membrane, the water is condensed and the dried permeate is analyzed by the mass spectrometer. The same type of samples is used here with 1 mm thick bulk BSCF5582 perovskitic membranes. Several steps with increasing humidity are measured, beginning from pure argon, going to higher water contents of 40.06, 50.06, 60.59, 72,75 and 85.75 vol. % H$_2$O. The exact water contents are determined considering the ideal gas law by calculating the volume flow rate of water

$$\dot{V}_{H_2O(g),T_2} = \frac{\dot{m}_{H_2O} \cdot R \cdot T_2}{p \cdot M_{H_2O}} \left[\frac{\text{m}^3}{\text{s}}\right] \tag{9}$$

and the carrier gas (argon) flow rate

$$\dot{V}_{CG,T_2} = \dot{V}_{CG,T_1} \cdot \frac{T_2}{T_1} \left[\frac{\text{ml}}{\text{min}}\right], \tag{10}$$

with $T_2 = 900\,°C$, $T_1 = 20\,°C$, the mass flow of liquid water $\dot{m}_{H_2O}$, the pressure $p = 1$ atm and the molecular weight of water M_{H_2O}. The water content w_{H_2O} is finally given by the equation

$$\dot{w}_{H_2O(g),T_2} = \frac{\dot{V}_{H_2O(g),T_2}}{\dot{V}_{H_2O(g),T_2} + \dot{V}_{CG,T_2}} \cdot 100 \ [\text{vol.\%}]. \tag{11}$$

Due to the increasing H_2O content, the total volume flow

$$\dot{V}_{total}^{900\,°C} = \dot{V}_{H_2O(g),T_2} + \dot{V}_{CG,T_2} \tag{12}$$

rises with increasing humidity level. According to this, the partial pressure p''_{O_2} at the back side becomes lower with higher water contents, resulting in a higher oxygen permeation rate in consequence of a higher Δp_{O_2}. The values for p''_{O_2} decrease from $4.1 \cdot 10^{-3}$ atm for 0 vol % H_2O to $1.63 \cdot 10^{-3}$ atm for 85.75 vol % H_2O. Fig. 5 shows the results of this first run.
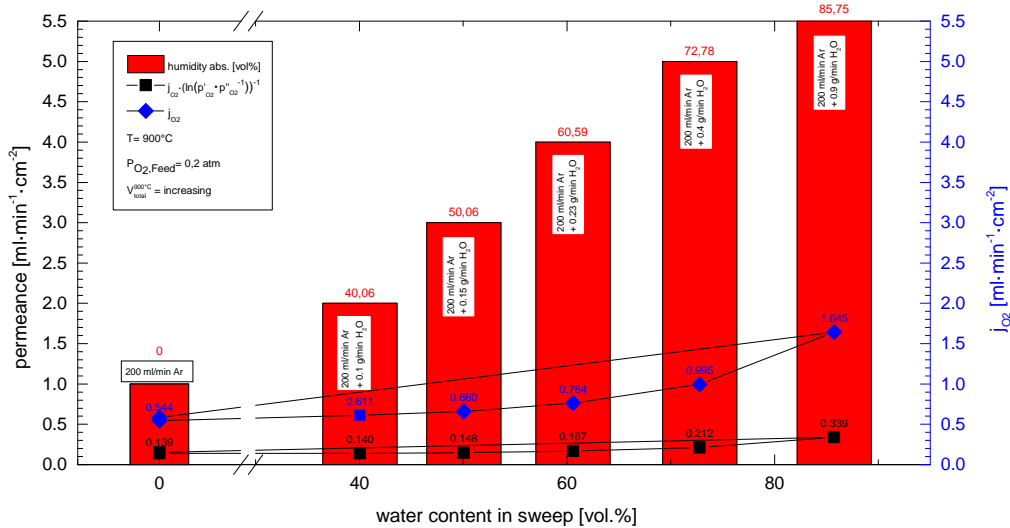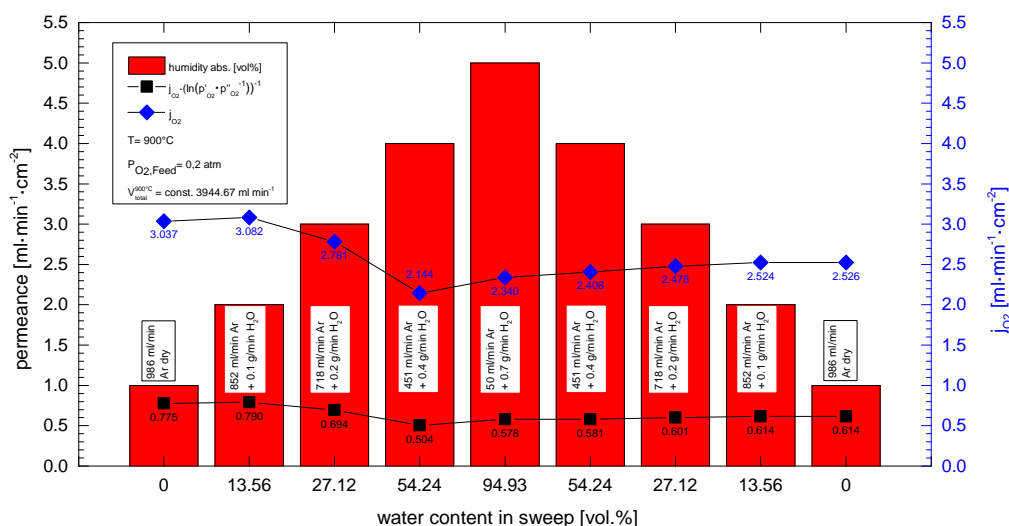

Figure 5. Permeation measurement at 900 °C with increasing amount of water added to a constant sweep volume of 200 ml min⁻¹ argon.

Herein, the permeance (7) and the permeation flux j_{O_2} (8) are plotted against the water content (11) in the sweep. The red bars indicate the level of humidity. Beginning from 0.139 ml min⁻¹ cm⁻² at dry conditions, the permeance increases with the amount of water in the sweep gas, reaching 0.339 ml min⁻¹ cm⁻² at 85.75 vol. %. $\dot{V}_{total}^{900\,°C}$ concurrently increases from $800 - 5600$ ml min⁻¹. The permeation flux j_{O2} is effected even more by higher volumes of added water. The values increase from 0.544 to 1.645 ml min⁻¹ with rising amount of steam. However, one can conclude from this data, that there are no permanent degradation effects, due to the fact that the permeation flux reaches the same level at dry conditions again, just as before steam contact. Concerning the leakage flux across the sealing we have calculated a nitrogen flux of about 15 % for dry conditions, which decreases with rising amount of water to approximately 5 %. Comparing the results of Fig. 5 with those of the 3-end temperature loop experiment in Fig. 4, the rate of about 0.8 ml min⁻¹ cm⁻² at similar conditions (1 mm

thick membranes; 900 °C) is slightly higher (approx factor 2.3) than the values in the vapor sweep experiment (Fig. 5). This indicates that a stronger partial pressure gradient Δp_{O_2}, induced by the 10 mbar vacuum in the permeate, results in a higher permeation flux.

Complementary to the experiment described above, a second measurement is performed, wherein $V_{total}^{900\,°C}$ is adjusted to a constant value of about 3945 ml min^{-1} during the whole experiment. Due to the

Figure 6. Permeation measurement at 900 °C with constant total volume flow.

fact, that the sweep rate influences the oxygen permeation performance, the total volume flow is fixed at a constant value to make a stand-alone assertion about the oxygen transport rate. This is technically realized by means of reducing the carrier gas flux individually when water is added. Starting from dry conditions (986 ml min^{-1} argon) the water content is increased stepwise from $13.56 - 94.93$ vol.% and back to dry carrier gas in a loop. Simultaneously, the carrier gas flow rate is decreased in the range of $852 - 50$ ml min^{-1}. Thereby, the amount of added water is shifted from $0.1 - 0.7$ g min^{-1}. Calculating the oxygen partial pressure at the membrane's permeate side gives no clear tendency, so the values are in the range of $p_{O_2}'' = 4.18 \cdot 10^{-3} - 2.98 \cdot 10^{-3}$ atm. The permeation rate is measured for only two hours at each step, to avoid long exposure times of the steam to the quartz glass tubes of the recipient. The oxygen flux, or rather the permeance (8), versus humidity level is plotted in Fig. 6. In this context, the permeation rate is not much affected by the steam. The values for the permeance remain in the range of about $0.8 - 0.5$ ml min^{-1} cm^{-2}, more or less independent of the amount of water vapor in the sweep. The lower values at the descending branch of the loop might be explained by means of microstructural or phase changes of the material and/or the deposition of silica phases on top of the membrane's surface. With regard to the leakage of nitrogen in the water loop experiment with maintained total volume flow (Fig. 6), we have also calculated the percental N_2 flux which rises with the amount of water in the sweep, and decreases again with dropping water content. In this particular case, the N_2 leakage flux varies between 2.77 % and 17.15 % for rising water contents of 0 to 95 vol.%, and decreases again to 1.49 % with falling water contents.

Indeed, we have seen from comparable long term annealing experiments, that SiO_2 is evaporating from the quartz glass tubes, when high amounts of water vapor are present at temperatures around 900 °C. The formation of volatile $SiO_2 \cdot 2.5 \cdot H_2O(g)$ is known to happen from Huggett and Piper [24]. This can be found as a deposit on the membrane surface after the experiments, which is blocking the oxygen exchange between the membrane and the gas phase. Moreover, phase transitions from the cubic perovskite structure to the hexagonal structure can occur upon water vapor contact. As a consequence the permeation rate might be affected by a long exposure of the membranes to water vapor. This has been proven in a long term permeation experiment at 900 °C with 80 vol.% water in the sweep gas and compressed air for feed gas. A cross section of the affected membrane surface is depicted in Fig. 7, which supports this hypothesis. To prevent the effect of silica phase formation, the inner sweep gas tubes have to be exchanged by alumina for further studies. Hence, the steam will not be in contact with quartz glass before entering the membrane's surface.
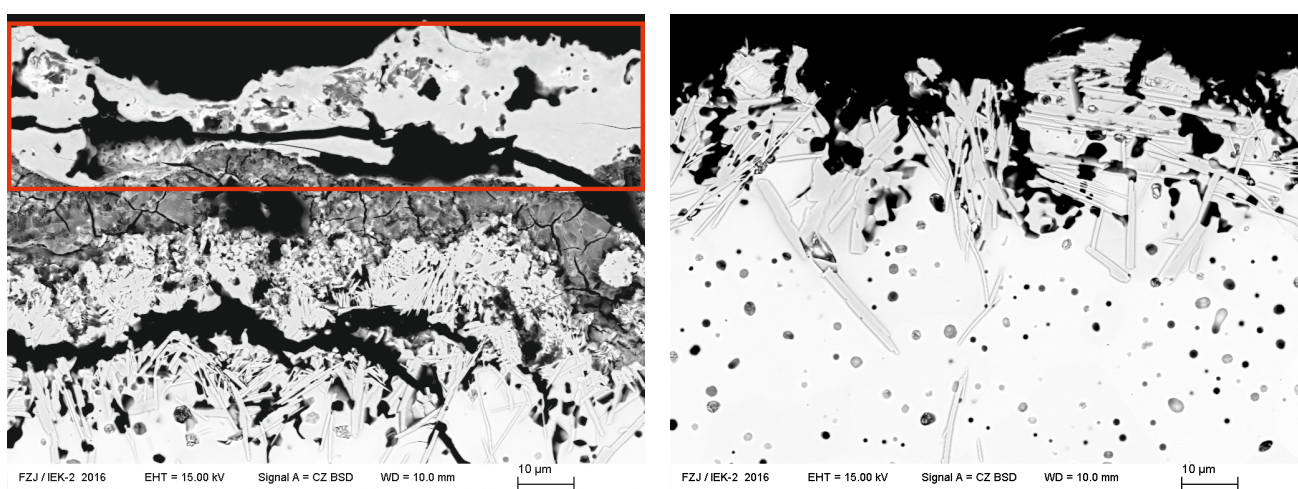
(a) Deposition of $10-20$ μm dense silica layer at the membrane surface.

(b) Crystallization of hexagonal phase needle-shaped structures.

Figure 7. SEM image of a 1 mm thick dense BSCF5582 membrane exposed to wet sweep gas ($0.8\,H_2O/0.2\,He$) for 384h at 900 °C.

4. Conclusions

In this study we have highlighted some aspects of the oxygen permeation performance of dense BSCF5582 membranes under different conditions, i.e. a temperature loop as well as varying steam concentrations in the sweep gas. The results reflect the assumptions of Wagner's theory (3) with a clear temperature dependence of the oxygen permeation. Moreover, the permeation rate is clearly affected by using steam for sweeping the back side of the membrane. We have shown that j_{O_2} is slightly increased by adding water vapor to the sweep gas, due to the continuously enlarged sweep volume flow. In case of a maintained total volume flow, j_{O_2} is not significantly affected by higher water contents. The SEM pictures of the long term permeation measurements under wet sweep conditions suggest morphological changes which could be partly responsible for degradation effects. This is resulting in a decreased oxygen exchange performance, which might be related to surface exchange

limited kinetics, accompanied by lowered permeation rates. However, the novelty of the investigation lies in the findings, that the observed degradation effects are for the most part reversible indicated by the measured oxygen fluxes after returning to dry conditions.

Acknowledgments

Conflict of Interest

All authors declare no conflicts of interest in this paper.

References

1. Czyperek M, Zapp P, Bouwmeester H, et al. (2010) Gas separation membranes for zero-emission fossil power plants: MEM-BRAIN. *J Membr Sci* 359: 149–159.

2. Smart S, Liu S, Serra J, et al. (2014) Perovskite membrane reactors: fundamentals and applications for oxygen production, syngas production and hydrogen processing. In: Gugliuzza A, Basile A, *Membranes for Clean and Renewable Power Applications*, 1 Eds., Cambridge, UK: Woodhead Publishing, 182–217.

3. Benson SJ, Waller D, Kilner JA (1999) Degradation of $La_{0.6}Sr_{0.4}Fe_{0.8}Co_{0.2}O_{3-\delta}$ in carbon dioxide and water atmospheres. *J Electrochem Soc* 146: 1305–1309.

4. Yi J, Feng S, Zuo Y, et al. (2005) Oxygen Permeability and Stability of $Sr_{0.95}Co_{0.8}Fe_{0.2}O_{3-}$ in a CO_2- and H_2O-Containing Atmosphere. *Chem Mater* 17: 5856–5861.

5. Yan A, Cheng M, Dong Y, et al. (2006) Investigation of a Ba0.5Sr0.5Co0.8Fe0.2O3 based cathode IT-SOFC: I. The effect of CO2 on the cell performance. *Appl Catal B* 66: 64–71.

6. Arnold M, Wang H, Feldhoff A (2007) Influence of CO_2 on the oxygen permeation performance and the microstructure of perovskite-type $(Ba_{0.5}Sr_{0.5})(Co_{0.8}Fe_{0.2})O_{3-\delta}$ membranes. *J Membr Sci* 293: 44–52.

7. Waindich A, Möbius A, Müller M (2009) Corrosion of $Ba_{1x}Sr_xCo_{1y}Fe_yO_{3-\delta}$ and $La_{0.3}Ba_{0.7}Co_{0.2}Fe_{0.8}O_{3-\delta}$ materials for oxygen separating membranes under Oxycoal conditions. *J Membr Sci* 337: 182–187.

8. Engels S, Markus T, Modigell M, et al. (2011) Oxygen permeation and stability investigations on MIEC membrane materials under operating conditions for power plant processes. *J Membr Sci* 370: 58–69.

9. Song CL, Yi JX (2015) Influence of CO_2 on Oxygen Surface Exchange Kinetics of Mixed-Conducting $Ba_{0.5}Sr_{0.5}Co_{0.8}Fe_{0.2}O_{3-\delta}$ Oxide. *Chinese J Chem Phys* 28: 203–205.

10. Wang H, Kölsch P, Schiestel T, et al. (2006) Production of high-purity oxygen by perovskite hollow fiber membranes swept with steam. *J Membr Sci* 284: 5–8.

11. Leo A, Liu S, Diniz da Costa JC (2011) Production of pure oxygen from BSCF hollow fiber membranes using steam sweep. *Sep Purif Technol* 78: 220–227.

12. Wang R, Meng B, Meng X, et al. (2015) Highly stable $La_{0.6}Sr_{0.4}Co_{0.2}Fe_{0.8}O_{3-\delta}$ hollow fibre membrane for air separation swept by steam or steam mixture. *J Membr Sci* 479: 232–239.

13. Wang Z, Kathiraser Y, Ang ML, et al. (2015) High Purity Oxygen Production via BBCN Perovskite Hollow Fiber Membrane Swept by Steam. *Ind Eng Chem Res* 54: 6371–6377.

14. Teraoka Y, Zhang H, Furukawa S, et al. (1985) Oxygen permeation through perovskite-type oxides. *Chem Lett* 14: 1743–1746.

15. Baumann S, Serra J, Lobera M, et al. (2011) Ultrahigh oxygen permeation flux through supported $Ba_{0.5}Sr_{0.5}Co_{0.8}Fe_{0.2}O_{3-\delta}$ membranes. *J Membr Sci* 377: 198–205.

16. Mogensen M, Sammes N, Tompsett G (2000) Physical, chemical and electrochemical properties of pure and doped ceria. *Solid State Ionics* 129: 63–94.

17. Ten Elshof J, Bouwmeester H, Verweij H (1995) Oxygen transport through $La_{1-x}Sr_xFeO_{3-\delta}$ membranes. I. Permeation in air/He gradients. *Solid State Ionics* 81: 97–109.

18. Sunarso J, Baumann S, Serra J, et al. (2008) Mixed ionicelectronic conducting (MIEC) ceramic-based membranes for oxygen separation. *J Membr Sci* 320: 13–41.

19. Shao Z, Yang W, Cong Y, et al. (2000) Investigation of the permeation behavior and stability of a $Ba_{0.5}Sr_{0.5}Co_{0.8}Fe_{0.2}O_{3-\delta}$ oxygen membrane. *J Membr Sci* 172: 177–188.

20. Serra J, Garcia-Fayos J, Baumann S, et al. (2013) Oxygen permeation through tape-cast asymmetric all-$La_{0.6}Sr_{0.4}Co_{0.2}Fe_{0.8}O_{3-\delta}$ membranes. *J Membr Sci* 447: 297–305.

21. Goldschmidt, V (1926) Die Gesetze der Krystallochemie. *Die Naturwissenschaften* 21: 477–485.

22. Bhalla, A, Ruyan G, and Rustum R (2000) The perovskite structure - a review of its role in ceramic science and technology. *Mater Res Innovations* 4: 3–26.

23. Bouwmeester H, Burggraaf A (1996) Chapter 10 – Dense ceramic membranes for oxygen separation. In: Burggraaf, A. J. and Cot, L. , *Membrane Science and Technology Series, 4*, Amsterdam, NL: Elsevier, 435–528.

24. Huggett L, Piper L (1966) Materials technology in steam reforming processes : proceedings (ed. C. Edeleanu). *Materials Technology Symposium Proceedings(1964 : Billingham Eng.)* Oxford ; New York : Symposium Publications Division, Pergamon Press, 337.